Iran J Sci Technol Trans Mech Eng (2020) 44:93–102
https://doi.org/10.1007/s40997-018-0242-1

RESEARCH PAPER

Impact Response of Thin Aluminium Plate with Varying Projectile Obliquity and Span Diameter

G. Tiwari[1] · M. A. Iqbal[2] · P. K. Gupta[2]

Received: 22 January 2016 / Accepted: 24 July 2018 / Published online: 31 July 2018

Abstract
This paper presents a three-dimensional (3-D) numerical investigation to know the effect of projectile obliquity and target span diameter on ballistic performance of 1-mm-thick target plate against ogive nosed projectile. The span diameter of 1100-H12 aluminium targets were varied as 68, 100, 150, 200 and 255 mm. Each span diameter of the target was impacted by ogive nosed projectile with varying angle of incidence as 0°, 10°, 20°, 30°, 40°,50° and 60° or till ricochet occurred. The numerical findings were validated through experiments for 0° projectile obliquity. Both the target span and angle of incidence of the projectile affected the mechanics of target deformation and its ballistic resistance significantly. The ballistic limit was found to be increased with increase in target span diameter as well as projectile obliquity. Moreover, the critical angle of ricochet also decreased with increase in target span diameter particularly at high incidence velocity.

Keywords Target span · Angle of incidence · Ogive nosed projectile · Ricochet

1 Introduction

Whenever collision between two bodies occurs, huge destruction as well as loss of life of human being occurs. To mitigate the damage, the proficient design of structures is necessary. In this context, the thin walled structure is widely used in military, civilian as well as industrial application due to their high stiffness and high strength to weight ratio. In the literature, many researchers addressed the mechanics of perforation (Awerbuch and Bodener 1973; Backman and Goldsmith 1978; Marom and Bonder 1979; Wilkins 1978; Liss et al. 1983; Corran et al. 1983), the influence of configuration (Marom and Bonder 1979; Iqbal et al. 2012; Dey et al. 2007; Wei et al. 2012; Yunfei et al. 2013) and thickness (Corran et al. 1983; Gupta et al. 2007) of the target as well as the influence of mass (Corran et al. 1983) and nose shape of the projectile (Iqbal et al. 2010a, 2012; Gupta et al. 2006, 2007; Arias et al. 2008) on the ballistic performance of the target.

In general, the projectile hits the target with some angle or obliquity. The angle of obliquity defined as the angle between the velocity vector of the projectile and the normal to the target surface (Backman and Goldsmith 1978). There are some studies which address the influence of the angle of the incidence of the projectile on the ballistic performance of the target. Based on oblique angle and projectile cone angle, the impact phenomenon was classified as low obliquity, high obliquity and very high obliquity (Zaid and Paul 1959). The forces generated during oblique impact were studied by Virostek et al. (1987) by impacting conical and hemispherical nosed projectile on steel as well as aluminium target. The angle of incidence was varied from 0° to 45°. For conical nosed projectile, the force generated increased with projectile incidence angle whereas opposite trend was found for hemispherical nosed projectile. In the similar way, the deformed shape of the target during oblique impact was studied by Johnson et al. (1982) through experiments on 50–100-mm-thick steel target against plasticine rod impact with obliquity of 0°–75°. Depth of crater in deformed target was found to be depending on velocity in that direction. The projectile oblique angle greater than 75° leads to ricochet of

✉ G. Tiwari
gauraviitdelhi@gmail.com

[1] Department of Mechanical Engineering, Visvesvaraya National Institute of Technology, Nagpur 440010, India

[2] Department of Civil Engineering, Indian Institute of Technology Roorkee, Roorkee 247667, India

projectile but when the projectile incidence velocity was found to be more than hydrodynamic transition velocity the projectile was found to be fragmented.

Goldsmith and Finnegan (1986) carried out an experimental investigation to study the ballistic behaviour of mild steel and aluminium targets impacted by blunt and conical projectile with the obliquity of 10°–50°. Velocity drop increased with the increase in plate thickness for both the material and became minimum in between 20° and 30°. At high velocity, more debris was produced particularly for mild steel targets. In the similar way, Yoo and Lee (2006) studied the behaviour of steel target against hemispherical nosed projectile impacted at 45°, 60° and 75° obliquity. The target offered the highest ballistic resistance when the ratio of plate oblique thickness to projectile diameter equals to two. Further Raguraman et al. (2008) studied the ballistic response of mild steel armour plate with varying thickness as 10, 12 and 16 mm. The brass jacketed steel hard core projectile obliquity was varied from 0 to 45°. Up to 30° obliquity the residual velocity remains same, thereafter decreases. In the similar way, Iqbal et al. (2010a, b) investigated the effect of projectile obliquity on monolithic and layered steel and aluminium target. The perforation behaviour of 12-mm-thick Weldox 460 E steel and 1-mm-thick 1100-H12 aluminium plate against conical and ogive nosed projectile with varying angle of incidence as 0°–60°. For 12-mm-thick steel target the ballistic limit was not changed up to 30° projectile obliquity, thereafter it increases drastically whereas for 1-mm-thick aluminium target ballistic limit increases consistently with projectile obliquity. Moreover, the angle of ricochet was also found to be increased with increase in incidence velocity for both the targets. The study was extended for layered target (2 × 6 mm steel, 2 × 0.5 mm aluminium) by Iqbal et al. (2010a). The ballistic limit was found higher for monolithic target compared to layered in contact target for all the projectile obliquity. Borvik et al. (2011) investigated the perforation phenomenon of 20-mm-thick AA6082-T4 aluminium target plate subjected to 7.62 × 63 mm NATO Ball and 7.62 × 63 mm APM2 projectile with varying angle of incidence as 0°, 15°, 30°, 45° and 60°. Against ball projectile, the residual velocity decreased consistently with projectile obliquity where as against APM 2 projectile the residual velocity unaffected up to 30° obliquity thereafter it decreased drastically.

There are very few studies that address the effect of target span on ballistic resistance (Iqbal et al. 2012; ABAQUS/Explicit user's manual 2007). Mannan et al. (2008) carried out an experimental investigation to know the behaviour of thin clamped aluminium beams of varying span to thickness ratio subjected to blunt nosed projectile impact. Three different failure modes i.e., Type I (fracture at the point of strike), Type II (fracture at one or both supports) and Type III (fracture at the point of strike with bulging and turn around supports after fracture) were observed and the expressions for corresponding threshold velocities were developed in terms of beam thickness (Mannan et al. 2008). In our previous study (Iqbal et al. 2012), the diameter of the 1-mm-thick aluminium target plate was varied from 50 to 500 mm against blunt and ogive nosed projectiles. The ballistic limit was significantly affected by span diameter for both the projectile.

The studies pertaining to the influence of target span are very limited and need to be further investigation. Further the influence of projectile obliquity on ballistic response of target of varying span diameter has not been addressed in the literature.

The present study deals with the three-dimensional numerical simulations of thin aluminium targets against ogive nosed projectiles with varying target span diameter and projectile obliquity. The diameter of 1-mm-thick 1100-H12 aluminium plate was varied as 68, 100, 150, 200 and 255 mm. The diameter and mass of the projectile was kept as 19 mm and 52.5 gm respectively. The projectile was impacted on each span diameter plate with varying angle of incidence as 0°, 10°, 20°, 30°, 40°,50° and 60° or till ricochet occurs. Experiments were also carried out wherein ogive nosed projectiles were normally (0° oblique angle) hit on 1-mm-thick 1100-H12 aluminium targets of 68, 100, 150,200 and 255 mm span diameter. At each target span diameter, the ballistic limit was obtained and the values thus obtained were compared with those obtained from the three-dimensional numerical simulation.

A consistent increase in the ballistic limit was found with increase in incidence angle of the projectile. The critical ricochet of the ogive nosed projectile occurred between 72° and 36° target obliquity in the considered velocity regimes and target span diameters. The critical angle of ricochet was found to increase with an increase in projectile impact velocity on the other hand it decreases with increase in target span diameter.

2 Experimental and Numerical Investigation

The experiments were carried out using a pressure gun consisting of a reciprocating compressor, a pressure cylinder, an automated actuator valve, a smooth long barrel, a mild steel target mounting plate and a projectile catcher, see Fig. 1. The impact and residual velocities of the projectile were measured with a high speed video camera, phantom V411.

Circular target plates of diameter 128, 160, 210, 260 and 315 mm were sandwiched between the 10-mm-thick steel mounting plate (with central hole) and 5-mm-thick steel ring through bolts. For 68 mm span diameter, six bolts

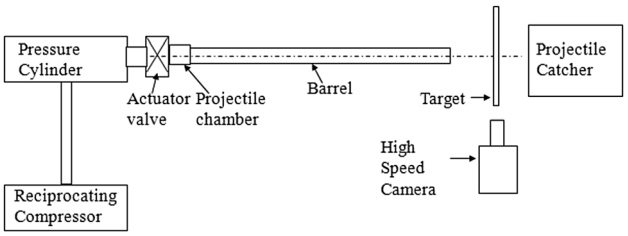

Fig. 1 Schematic diagram of pressure gun

whereas for other span diameter 8 bolts were arranged on a 98, 130, 180, 230 and 285 mm pitch circle diameter on the steel rings of 30 mm width. Thus the free span of aluminium plate was kept as 68, 100, 150, 200 and 255 mm as used in numerical study. A typical clamping arrangement and corresponding numerical model for 68 mm and 150 mm are shown in Fig. 2. After perforation, the projectile was recovered from a catcher. The catcher was filled with cotton rag to avoid damaging the projectile.

The 1100-H12 aluminium plates of 1 mm thickness were impacted by ogive nosed projectiles of 19 mm diameter, 50.8 mm length and 52.5 gm mass. The projectiles were made of EN-24 steel. For hardening these were oil quenched to Rockwell hardness Rc 47–52. For numerical simulation, three-dimensional finite element model of the projectile and target was made using ABAQUS/CAE (2007). Figure 3 shows a typical finite element model of the projectile and target, which were modelled as rigid and deformable body, respectively. The span diameter of the target was varied as 68, 100, 150, 200 and 255 mm same as in experiments. The oblique impact were simulated by rotating the target about its in-plane horizontal axis with 10°, 20°, 30°, 40°, 50° and 60° to get inclinations at desired angles. The kinematic contact algorithm was used to define the contact between the projectile and target. The outer surface of the projectile was modelled as the master surface and the contact region of the target as node based slave surface. In case of oblique impact, larger portion of the target was considered as node based slave surface.

With increase in projectile incidence angle, the region of target contact increases becomes largest for ricochet. The periphery of the target was restrained in all direction. The eight node brick elements with reduced integration were considered to model the target. A mesh convergence study was performed (Iqbal et al. 2012) wherein 1-mm-thick aluminium target with varying number of elements (3–7) across the thickness direction were impacted by ogive nosed projectile. The residual velocity increased up to five element in thickness direction thereafter it became constant. Therefore, six elements in thickness direction were

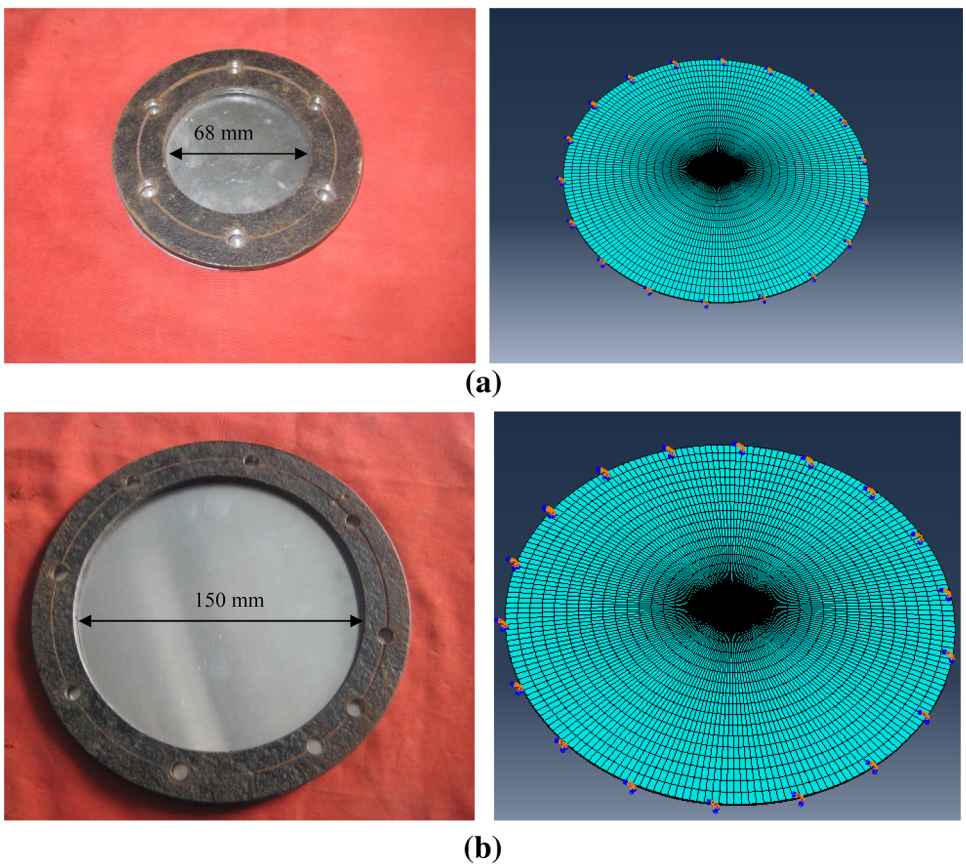

Fig. 2 Experimental and numerical model for target span diameter **a** 68 mm **b** 150 mm

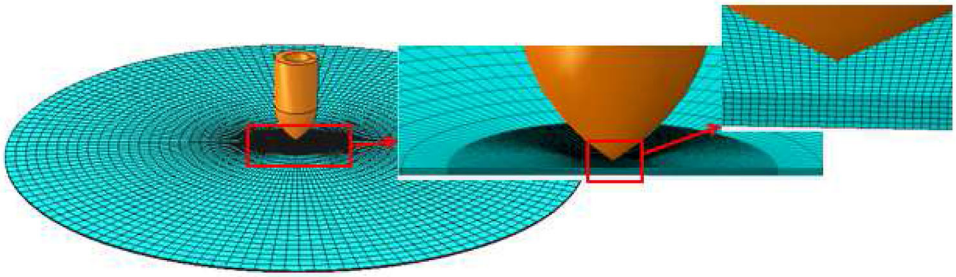

Fig. 3 Finite element model of target and projectile

considered for meshing the contact zone. The target with 68, 100, 150, 200 and 255 mm span diameter were meshed with 137,811, 152,643, 182,307, 204,555 and 256,467 elements.

3 Constitutive Modelling of the Target Material

During impact the material undergoes through yielding, plastic flow, strain hardening, strain rate hardening, softening due to adiabatic heating and damage simultaneously. The constitutive modelling of the material behaviour of 1100-H12 aluminium target in the present numerical simulation has been done using the Johnson–Cook elasto-viscoplastic material model (Johnson and Cook 1983, 1985) that is capable of incorporating the above processes. The equivalent von-Mises stress $\bar{\sigma}$ in the Johnson–Cook model is expressed as;

$$\bar{\sigma}\left(\bar{\varepsilon}^{\mathrm{pl}}, \dot{\bar{\varepsilon}}^{\mathrm{pl}}, \hat{T}\right) = \left[A + B\left(\bar{\varepsilon}^{\mathrm{pl}}\right)^{n}\right]\left[1 + C\ln\left(\frac{\dot{\bar{\varepsilon}}^{\mathrm{pl}}}{\dot{\varepsilon}_0}\right)\right]\left[1 - \hat{T}^{m}\right] \tag{1}$$

where A, B, n, C and m are material parameters. $\bar{\varepsilon}^{\mathrm{pl}}$ is equivalent plastic strain, $\dot{\bar{\varepsilon}}^{\mathrm{pl}}$ is equivalent plastic strain rate, $\dot{\varepsilon}_0$ is a reference strain rate and $\hat{T}$ is non dimensional temperature defined as;

$$\hat{T} = (T - T_0)/(T_{\mathrm{melt}} - T_0) \quad T_0 \le T \le T_{\mathrm{melt}} \tag{2}$$

where T is the current temperature, T_{melt} is the melting temperature and T_0 is the room temperature.

The failure is assumed to occur when the damage parameter D exceeds unity. This parameter D is expressed as:

$$D\left(\bar{\varepsilon}^{P}, \dot{\bar{\varepsilon}}^{P}, T, \sigma^{*}\right) = \sum \frac{\Delta\bar{\varepsilon}^{P}}{\bar{\varepsilon}_{\mathrm{f}}^{P}\left(\dot{\bar{\varepsilon}}^{P}, T, \sigma^{*}\right)} \tag{3}$$

where, $\Delta\bar{\varepsilon}^{P}$ is an increment of accumulated equivalent plastic strain that occurs during an integration cycle and $\bar{\varepsilon}_{\mathrm{f}}^{P}$ is the critical failure strain.

The fracture model proposed by Johnson–Cook (Johnson and Cook 1985) takes into account the effect of triaxial state of stress, strain rate and temperature on the equivalent fracture strain. The equivalent fracture strain $\bar{\varepsilon}_{\mathrm{f}}^{P}$ is expressed as;

$$\bar{\varepsilon}_{\mathrm{f}}^{\mathrm{pl}}\left(\frac{\sigma_{\mathrm{m}}}{\bar{\sigma}}, \dot{\bar{\varepsilon}}^{\mathrm{pl}}, \hat{T}\right) = \left[D_1 + D_2\exp\left(D_3\frac{\sigma_{\mathrm{m}}}{\bar{\sigma}}\right)\right]\left[1 + D_4\ln\left(\frac{\dot{\bar{\varepsilon}}^{\mathrm{pl}}}{\dot{\varepsilon}_0}\right)\right]\left[1 + D_5\hat{T}\right] \tag{4}$$

where $D_1 - D_5$ are material parameters, $\frac{\sigma_{\mathrm{m}}}{\bar{\sigma}}$ is the stress triaxiality ratio and σ_{m} is the mean stress. The material parameters for 1100-H12 aluminium alloy were determined (Gupta et al. 2006) as follows and are given in Table 1.

4 Results and Discussion

The results of the present experimental and numerical study has been shown in Tables 2, 3, 4, 5 and 6 in the form of impact and residual velocities for 68, 100, 150, 200 and

Table 1 Material parameters for 1100-H12 aluminium target (Gupta et al. 2006)

Modulus of elasticity, E (N/mm^2)	65,762
Poison's ratio, v	0.3
Density, ρ (kg/m^3)	2700
Yield stress, A (N/mm^2)	148.361
B (N/mm^2)	345.513
n	0.183
Reference strain rate, $\dot{\varepsilon}_0$ (s-1)	1.0
C	0.001
m	0.859
T_{melt} (K)	893
T_0 (K)	293
Specific heat, Cp (J/kg-K)	920
Inelastic heat fraction, α	0.9
$D1$	0.071
$D2$	1.248
$D3$	− 1.142
$D4$	0.0097
$D5$	0.0

Table 2 Experimental and numerical results for ballistic resistance of 68 mm span diameter

Target thickness = 1 mm, ogive nosed projectile (mass = 52.5 grams, diameter = 19 mm)									
Target span diameter (mm)	Impact velocity (m/s)	Residual velocity (m/s)							
		Obliquity							
		0° (normal impact)		10°	20°	30°	40°	50°	60°
		Experimental	Numerical						
68	109.09	100	101.74	100.86	100.49	99.89	97.36	35.93	93.21
	100	85.71	91.91	90.83	90.76	90.02	87.21	85.7	67.37
	92.3	78.94	83.27	82.10	81.2	80.32	78.03	76.3	30.37
	70.58	55.55	57.88	56.24	56.16	53.7	51.3	44.7	Ricochet
	64.28	51.72	52.04	48.07	48.11	45.77	42.00	31.8	–
	53.0	–	–	–	–	–	10.2	6.2	–
	48.62	25.72	26.23	25.00	21.8	14.3	0	0	–
	46.25	–	–	–	–	3.5	–	–	–
	43.5	–	–	–	–	0	–	–	–
	43.15	–	–	–	6.2	–	–	–	–
	41.91	0	14.3	10.9	–	–	–	–	–
	41.0	–	–	–	0	–	–	–	–
	40.52	–	8.7	0	–	–	–	–	–
	38.5	–	0	–	–	–	–	–	–

Table 3 Experimental and numerical results for ballistic resistance of 100 mm span diameter

Target thickness = 1 mm, ogive nosed projectile (mass = 52.5 gm, diameter = 19 mm)									
Target span diameter (mm)	Impact velocity (m/s)	Residual velocity (m/s)							
		Projectile obliquity							
		0° (normal impact)		10°	20°	30°	40°	50°	60°
		Experimental	Numerical						
100	102.61	94.05	93.87	92.71	92.3	91.10	89.2	87.3	86.4
	89.78	80.15	79.66	78.6	78.04	77.1	74.6	71.16	69.7
	85.70	75.0	75.04	73.95	73.48	72.60	69.3	66.03	64.7
	76.95	70.53	65.1	63.7	63.68	62.7	58.3	54.3	Ricochet
	60.17	45.96	43.29	43.5	43.3	38.8	32.02	13.9	–
	58.50	–	–	–	–	–	–	Ricochet	–
	55.00	–	–	–	–	–	19.9	–	–
	46.15	20.0	21.93	18.8	16.4	7.6	Ricochet	–	–
	45.50	–	–	–	–	0	–	–	–
	42.85	0	14.02	8.2	4.5	–	–	–	–
	42.30	–	–	–	0	–	–	–	–
	41.05	–	–	0	–	–	–	–	–
	38.5	–	0	–	–	–	–	–	–

255 mm target span diameters respectively. For normal impact, a close correlation of residual velocities of the projectiles was observed between the results of experiments and numerical simulations. The effect of span did not appear at high projectile incidence velocity while close to ballistic limit it became much significant. The

Table 4 Experimental and numerical results for ballistic resistance of 150 mm span diameter

Target thickness = 1 mm, ogive nosed projectile (mass = 52.5 gm, diameter = 19 mm)									
Target span diameter (mm)	Impact velocity (m/s)	Residual velocity (m/s)							
		Projectile obliquity							
		0° (normal impact)		10°	20°	30°	40°	50°	60°
		Experimental	Numerical						
150	104.00	97.05	94.77	93.94	93.22	91.71	88.7	86.7	82.35
	97.06	85.64	87.1	86.11	85.49	83.3	80.38	78.4	72.5
	79.42	65.51	66.5	64.9	64.73	61.4	58.1	57.36	Ricochet
	70.00	50.0	54.64	52.80	52.73	48.90	46.39	35.70	–
	64.28	42.85	47.70	45.30	45.33	41.80	36.5	–	
	60.00	–	–	–	–	–	28.18	–	–
	55.26	32.92	34.87	32.6	–	29.01	Ricochet	–	–
	52.50	27.77	29.50	28.47	28.40	–	–	–	–
	50.00	26.47	27.74	25.34	21.3	18.7	–	–	–
	47.50	–	–	–	–	7.8	–	–	–
	45.00	–	–	–	–	0	–	–	–
	44.15	–	–	–	9.2	–	–	–	–
	43.5	–	–	6.8	0	–	–	–	–
	42.5	–	4.5	–	–	–	–	–	–
	42.15	–	–	–	–	–	–	–	–
	41.15	–	–	0	–	–	–	–	–
	40.05	0	0	–	–	–	–	–	–

Table 5 Experimental and numerical results for ballistic resistance of 200 mm span diameter

Target thickness = 1 mm, ogive nosed projectile (Mass = 52.5 gm, diameter = 19 mm)									
Target span diameter (mm)	Impact velocity (m/s)	Residual velocity (m/s)							
		Projectile obliquity							
		0° (normal impact)		10°	20°	30°	40°	50°	60°
		Experimental	Numerical						
200	108.08	96.07	99.11	98.37	97.70	95.53	93.30	91.33	74.40
	96.00	82.35	85.70	84.84	84.15	81.51	78.20	75.80	Ricochet
	78.61	61.76	65.07	63.73	63.30	59.81	54.40	51.20	–
	66.52	48.04	49.30	47.47	47.3	41.60	35.20	27.03	–
	52.94	29.11	27.70	24.50	24.20	14.40	6.7	Ricochet	–
	51.15	–	–	–	–	10.4	0	–	–
	48.50	–	–	–	–	0	–	–	–
	46.59	0	16.3	–	–	–	–	–	–
	45.50	–	–	–	5.5	–	–	–	–
	44.3	–	–	7.3	0	–	–	–	–
	43.05			0					
	42.50		3.6						
	42.15		0						

Table 6 Experimental and numerical results for ballistic resistance of 255 mm span diameter

Target thickness = 1 mm, ogive nosed projectile (mass = 52.5 gm, diameter = 19 mm)									
Target span diameter (mm)	Impact velocity (m/s)	Residual velocity (m/s)							
		Projectile obliquity							
		0° (normal impact)		10°	20°	30°	40°	50°	60°
		Experimental	Numerical						
255	81.03	70.89	67.1	66.66	66.13	62.51	58.59	53.06	Ricochet
	72.46	58.01	55.53	55.45	55.00	50.19	45.25	35.2	–
	70.89	54.02	53.6	53.34	52.90	47.77	42.25	30.76	–
	55.00	–	–	26.79	26.36	10.3	6.9	Ricochet	–
	54.00	–	–	–	–	–	0	–	–
	50.00	–	–	14.6	10.5	0	–	–	–
	47.50	–	–	–	0	–	–	–	–
	45.25	–	4.9	–	–	–	–	–	–
	42.46	8.41	0	0	–	–	–	–	–
	41.40	0	–	–	–	–	–	–	–

Table 7 Ballistic limit of the targets

Target span diameter (mm)	Ballistic limit (V_{50} m/s)				
	Ogive nosed projectile obliquity				
	0°		10°	20°	30°
	Experimental	Numerical			
68	42.77	39.51	41.2	42.05	44.87
100	43.60	40.67	41.95	42.60	45.80
150	45.03	41.27	42.32	43.15	46.25
200	45.44	42.32	43.67	44.90	49.83
255	46.45	43.85	46.23	48.75	52.50

targets having larger span diameter provide more resistance against projectile motion. The effect of projectile obliquity was more significant at low projectile incidence velocity. Table 7 shows the ballistic limit velocity obtained through experiments (for normal impact) and numerical simulations (0°, 10°, 20° and 30° obliquity) of the target for different target span diameter. The ballistic limit velocities have been calculated as the average of the highest velocity giving no perforation and the lowest velocity giving complete perforation of the target, V_{50}.

Table 8 Variation in angle of ricochet with target span diameter and impact velocities

Target span diameter (mm)	Impact velocity (m/s)				
	109.09	92.3	70.58	55.2	46.5
	Critical angle of ricochet (°)				
68	72	67	59	52	45
100	71	63	56	47	40
150	67	60	53	45	36
200	62	57	52	45	36
255	59	56	52	45	36

The ballistic limit was found to increase with an increase in target span diameter. The reason behind this behaviour was observed as higher global deformation of the target for larger span diameter. The kinetic energy of the projectile dissipates in plastic deformation of the target and residual kinetic energy of the projectile. Close to ballistic limit the energy dissipated in target deformation becomes highest (Corran et al. 1983). Moreover, the ballistic limit increased with increase in angle of incidence of the projectile. For the oblique angle more than 30° the ballistic limit was not clear due to occurrence of ricochet. For normal impact the actual ballistic limit increased by 1.9, 5.3, 6.2 and 8.6%, respectively, for the target with 100, 150, 200 and 255 mm span diameter when compared to 68 mm span diameter whereas corresponding predicted values were as 2.9, 4.5, 7.1 and 11%. Similarly for 10°

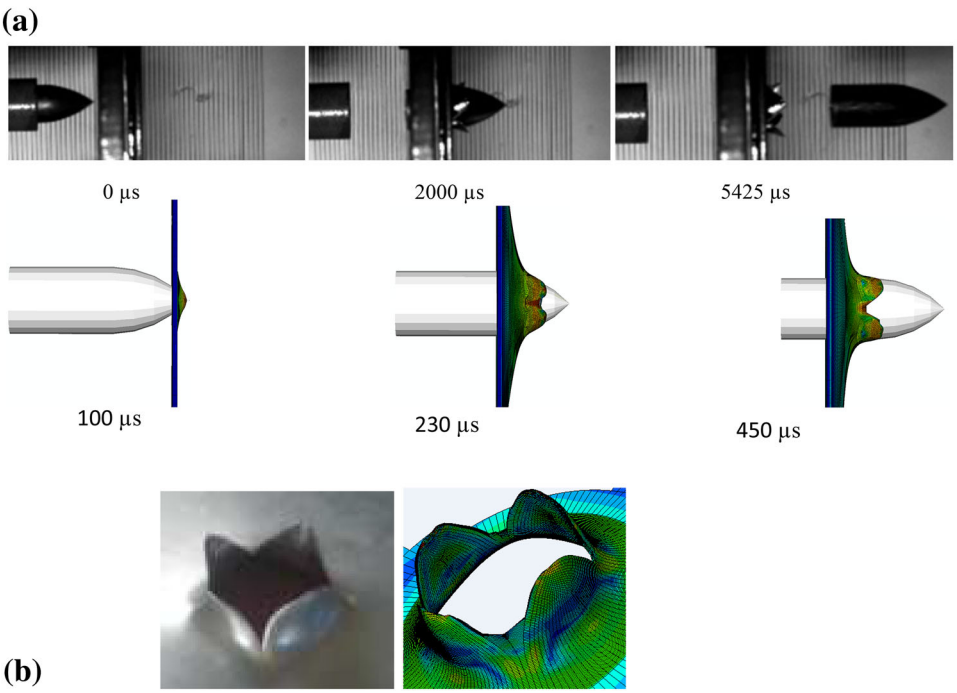

Fig. 4 Observed and predicted **a** perforation phenomenon of target of 150 mm span diameter subjected to normal impact of ogive nosed projectile at 52.5 m/s **b** failure mode

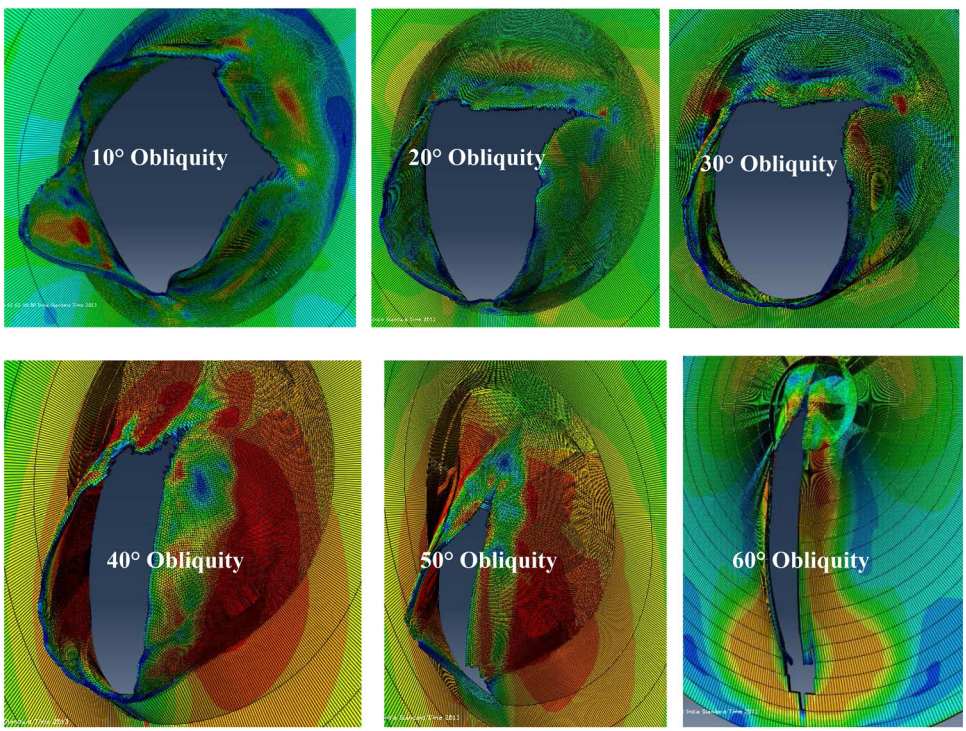

Fig. 5 Failure modes of 1-mm-thick 1100-H12 aluminium target at different obliquities

projectile obliquity the increase in predicted ballistic limit was found as 1.8, 2.7, 6 and 12.2%, for 20° projectile obliquity it was 1.3, 2.6, 6.7 and 15.9% and for 30° projectile obliquity it was 2.07, 3.07 11.04 and 17% for target span diameter of 100, 150, 200 and 255 mm. For each span diameter the ballistic limit increase with projectile obliquity. When projectile incidence angle increased by 0°–30°, the ballistic limit increased by 13.7, 12.6, 12.05, 17.7 and 19.7% for target span diameter 68, 100, 150, 200 and 255 mm, respectively.

Table 8 shows the effect of projectile incidence velocity and target span diameter on critical angle of ricochet. The effect of span on critical angle of ricochet was investigated for different range of projectile incidence velocity (109.09,

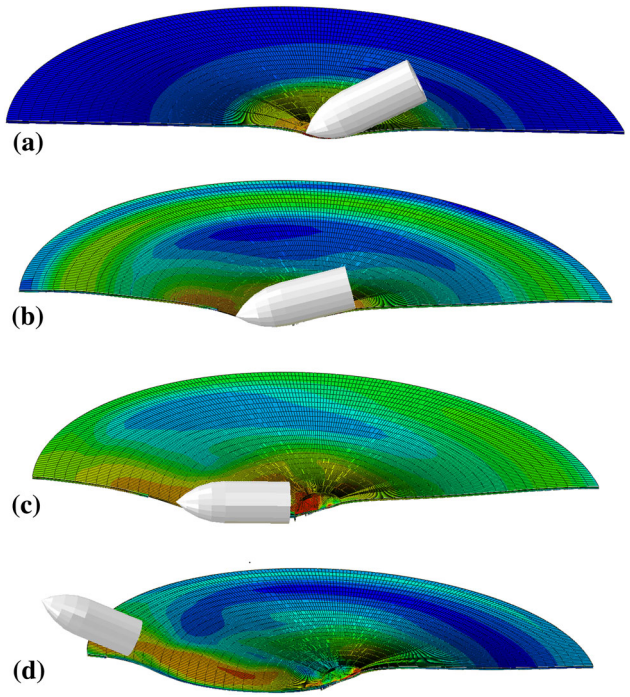

Fig. 6 Critical ricochet of ogive nosed projectile impacted on 1-mm-thick 1100-H12 aluminium target at 59° obliquity and 109 m/s velocity

92.3, 70.58, 55.2 and 46.5 m/s). The critical angle of ricochet was found to increase with increase in target span diameter particularly at high projectile incidence velocity. The increase in critical angle of ricochet was more prominent when target span diameter increased from 68 to 150 mm. At low projectile incidence velocity the critical angle of ricochet became constant for the target span diameter 150, 200 and 255 mm. Moreover, for same projectile incidence velocity a significant decrease in critical angle of ricochet was found with target span diameter. The critical angle of ricochet decreased from 72° to 59° when target span diameter increased from 68 to 255 mm at 109.09 m/s projectile incidence velocity, while at 46.5 m/s the critical angle of ricochet decreases from 45° to 36°.

The progress of deformation and perforation phenomena is shown in Fig. 4a. When a sharp nosed projectile hits the plate, initial crack appears at the contact region due to compressive stresses. These cracks subsequently propagate in the outward direction due to high radial and circumferential tensile stresses as the ogival nose perforates the target. This phenomenon also causes the development of petals and due to further movement of projectile the petal bends in rear direction as shown in Fig. 4a. Figure 4b shows the experimental and numerical results of the failure modes of the plate against normal impact of ogive nosed projectile. Four equal size petals were formed in the target subjected to normal impact by ogive nosed projectile, see Fig. 4b. The failure mechanism of the target remained unaffected by target span diameter but significantly altered with the projectile incidence angle.

Figure 5 shows the failure mode of the target against different projectile obliquity. The angle of incidence of the projectile was significantly affected the mechanics of failure. The failure of the target occurred through petal formation at each angle of impact. Under a normal impact, a circular hole of diameter equal to that of the projectile is formed along with four equal petals. In the case of oblique impact the hole is elliptic and the four petals are unequal in size. The size of upper two petals decreases and that of the lower two petals increases with increase in obliquity.

Figure 6 shows the critical ricochet of ogive nosed projectile as a result of impact on an aluminium target at 59° obliquity and 109.09 m/s velocity. In this case the projectile hit the target at initial obliquity and deformed the contact region significantly. The projectile also started deviating from its central axis away from the plate normal. The projectile slid over the surface of the target and finally rebounded back from the front surface after deviating almost 90° from its central axis.

5 Conclusions

The effect of the extent of projectile incidence angle along with target span on the mechanics of deformation and ballistic resistance of 1-mm-thick 1100-H12 aluminium plates were studied when subjected to the impact of an ogive nosed projectile. The experiments were carried out using a pressure gun while the numerical simulations were performed through ABAQUS/Explicit finite element code. The target span diameter was varied as 68, 100, 150, 200 and 255 mm. Each target span was impacted by the ogive nosed projectile with varying incidence angle as 0°, 10°, 20°, 30°, 40°, 50° and 60°. Further, the effect of span and projectile incidence velocity on critical angle of ricochet was investigated.

The ballistic limit of the target of 100, 150, 200 and 255 mm span diameter, increased by 2.9, 4.5, 7.1 and 10.9%, respectively, as compared to that of the target of 68 mm span diameter. The target offered higher ballistic limit against oblique impact of the projectile as compared to normal impact. Moreover, this effect was more prominent for larger span diameter. The increase in angle of incidence of the projectile from 0° to 30° caused an increase in ballistic limit as 13.7, 12.6, 12.05, 17.7 and 19.7% for 68, 100, 150, 200 and 255 mm target span diameter, respectively.

The critical angle of ricochet increased with projectile incidence velocity. The critical angle of ricochet increased by 60, 77.5, 86.1, 72.2 and 63.8% for the 68, 100, 150, 200

and 255 mm target span diameter when the projectile incidence velocity increases from 46.5 to 109.09 m/s. Further the critical angle of ricochet decreased with increase in target span diameter particularly at high projectile incidence velocity.

References

ABAQUS/Explicit user's manual (2007) Version 6.7, 1(2)

Arias A, Rodríguez-Martínez JA, Rusinek A (2008) Numerical simulations of impact behaviour of thin steel plates subjected to cylindrical, conical and hemispherical non-deformable projectiles. Eng Fract Mech 75:1635–1656

Awerbuch J, Bodener SR (1973) Analysis of the mechanics of perforation of projectile in metallic plates. Int J Solids Struct 10:671–684

Backman ME, Goldsmith W (1978) The mechanics of penetration of projectile into targets. Int J Eng Sci 16:1–99

Borvik T, Olovsson L, Dey S, Langseth M (2011) Normal and oblique impact of small arms bullets on AA6082-T4 aluminium protective plates. Int J Impact Eng 38:577–589

Corran RSJ, Shadbolt PJ, Ruiz C (1983) Impact loading of plates—an experimental investigation. Int J Impact Eng 1:3–22

Dey S, Borvik T, Teng X, Wierzbicki T, Hopperstad OS (2007) On the ballistic resistance of double-layered steel plates: an experimental and numerical investigation. Int J Solids Struct 44:6701–6723

Goldsmith W, Finnegan SA (1986) Normal and oblique impact of cylindro-conical and cylindrical projectiles on metallic plates. Int J Impact Eng 4–2:83–105

Gupta NK, Iqbal MA, Sekhon GS (2006) Experimental and numerical studies on the behaviour of thin aluminium plates subjected to impact by blunt- and hemispherical nosed projectiles. Int J Impact Eng 32:1921–1944

Gupta NK, Iqbal MA, Sekhon GS (2007) Effect of projectile nose shape, impact velocity and target thickness on deformation behaviour of aluminium plates. Int J Solids Struct 44:3411–3439

Iqbal MA, Gupta G, Diwakar A, Gupta NK (2010a) Effect of projectile nose shape on the ballistic resistance of ductile targets. Euro J Mech A/Solids 29:683–694

Iqbal MA, Gupta G, Gupta NK (2010b) 3D numerical simulations of ductile targets subjected to oblique impact by sharp nosed projectiles. Int J Solids Struct 47:224–237

Iqbal MA, Gupta PK, Deore VS, Tak SK, Tiwari G, Gupta NK (2012) Effect of target span and configuration on the ballistic limit. Int J Impact Eng 42:11–24

Johnson GR, Cook WH (1983) A constitutive model and data for metals subjected to large strains, high strain rates and high temperatures. In: Proceedings of the seventh international symposium on ballistics, The Hague

Johnson GR, Cook WH (1985) Fracture characteristics of three metals subjected to various strains, strain rates, temperatures and pressures. Eng Fract Mech 21(1):31–48

Johnson W, Sengupta AK, Ghosh SK (1982) Plasticine modelled high velocity oblique impact and ricochet of long rods. Int J Mech Sci 24–7:437–455

Liss J, Goldsmith W, Kelly JM (1983) A phenomenological penetration model of plates. Int J Impact Eng 1:321–341

Mannan MN, Ansari R, Abbas H (2008) Failure of aluminium beams under low velocity impact. Int J Impact Eng 35:1201–1212

Marom I, Bonder SR (1979) Projectile perforation of multi-layered beams. Int J Mech Sci 21:489–504

Raguraman M, Deb A, Gupta NK (2008) A simulation-driven study of oblique impact of ogival-nosed projectiles on mild steel armour plates. Latin Am J Solids Struct 5:225–235

Virostek SP, Dual J, Goldsmith W (1987) Direct force measurement in normal and oblique impact of plates by projectiles. Int J Impact Eng 6:247–269

Wei Z, Yunfei D, Zongsheng C, Gang W (2012) Experimental investigation on the ballistic performance of monolithic and layered metal plates subjected to impact by blunt rigid projectiles. Int J Impact Eng 49:115–129

Wilkins ML (1978) Mechanics of Penetration and perforation. Int J Impact Eng 16:793–807

Yoo YH, Lee M (2006) Protection effectiveness of an oblique plate against a long rod. Int J Impact Eng 33:872–879

Yunfei D, Wei Z, Zongsheng C (2013) Experimental investigation on the ballistic resistance of monolithic and multi-layered plates against ogival-nosed rigid projectiles impact. Mat Des 44:228–239

Zaid M, Paul B (1959) Oblique perforation of a thin plate by a truncated conical projectile. J Frankl Inst 268:24–45